Acta Cryst. (1982). B38, 6–15

Bonding in a Binuclear Metal Carbonyl: Experimental Charge Density in $Mn_2(CO)_{10}$

BY MICHEL MARTIN, BERNARD REES* AND ANDRÉ MITSCHLER

Institut le Bel, Université Louis Pasteur, 4 Rue Blaise Pascal, 67070 Strasbourg CEDEX, France

(*Received* 10 *December* 1980; *accepted* 6 *May* 1981)

Abstract

X-ray diffraction data (Ag $K\alpha$ and Mo $K\alpha$ radiation) have been collected at 74 K on dimanganese decacarbonyl $Mn_2(CO)_{10}$, and the crystal structure was refined. The atomic positional and thermal parameters were determined from high-angle Ag $K\alpha$ data to avoid systematic errors due to bonding effects. The molecular geometry is discussed. The distortions are larger than at room temperature: for example, the torsion angle of the two $Mn(CO)_5$ fragments is 50·2°, compared to 47·4° at room temperature, and 45° for an ideal D_{4d} symmetry. '$X-X$' deformation-density maps were computed and averaged over chemically equivalent sites. No significant charge-density accumulation is observed on the Mn–Mn bond. The configuration around the Mn atoms is essentially octahedral, with about 75% of the $3d$ electrons in the diagonal orbitals (d_{xy},d_{xz},d_{yz}) and the remaining 25% in d_{z^2} and $d_{x^2-y^2}$. Atomic charges were determined both by direct integration and by least-squares refinement. Directly integrated charges are very small. Mn seems slightly negative. Both methods of charge integration show a clear difference between axial and equatorial carbonyls, which is confirmed by comparing their electron density with that of free carbon monoxide: the differences are characteristic of a σ-bonding π-backbonding mechanism, and are larger for the axial carbonyls than for the equatorial carbonyls. This confirms the stronger bonding of the axial carbonyls, also responsible for the longer C–O bond and the shorter Mn–C bond.

Introduction

Dimanganese decacarbonyl has been the subject of many experimental and theoretical investigations. Work has been published in different experimental fields, including X-ray diffraction (Dahl & Rundle, 1963), electron diffraction in the vapour phase (Almenningen, Jacobsen & Seip, 1969) and a number of thermodynamic and spectroscopic investigations. Quantum chemical calculations have been performed by extended Hückel-type methods (Brown, Chambers, Fitzpatrick & Rawlinson, 1971; Levenson & Gray, 1975; McKinney & Pensak, 1979), by extended CNDO (Savariault, 1978; Freund, Dick & Hohlneicher, 1980) and by the Hartree–Fock–Slater (HFS-Xα) method (Heijser, Baerends & Ros, 1980), the latter probably being the closest to an *ab initio* calculation. This enumeration is not exhaustive, but illustrates the interest in this compound, which is mostly due to the Mn–Mn bond, $Mn_2(CO)_{10}$ being one of the simplest compounds with a metal–metal bond. A single bond is required to account for the diamagnetic behaviour and to obey the 18-electron rule. The radiocrystallographic investigation has shown that this bond is very long, 2·92 Å, about 0·5 Å more than the sum of the covalent radii (Dahl & Rundle, 1963) and not supported by carbonyl bridges. However, the four equatorial carbonyls on each Mn atom are slightly bent toward the other Mn atom and this has been considered as an indication of partial bridging (Brown *et al.*, 1971; Bau, Kirtley, Sorrell & Winarko, 1974): taking the z axis along the Mn–Mn bonds, bending of the carbonyls would enhance the overlap between the π^* orbitals and the $3d_{xz}$ (or $3d_{yz}$) orbital of the other Mn atom, giving rise to a backbonding interaction between the metal and ligands not directly bonded to it. This bending, however, could also be due to steric interaction between the axial and equatorial carbonyls. This view is supported by the crystal structure of $HMn(CO)_5$, in which even larger bending is observed, and no metal–carbonyl cross-interaction can be invoked (La Placa, Hamilton, Ibers & Davison, 1969).

While Brown *et al.* (1971) conclude, on grounds of energy considerations and Mulliken populations, that cross-interaction between carbonyls and the metal of the other $Mn(CO)_5$ group plays an essential role in the metal–metal bonding, Heijser *et al.* (1980) find no evidence of it from the results of their HFS calculation: the interaction between the metal $3d_{xz}$ or $3d_{yz}$ orbitals and the carbonyl π^* orbitals is concentrated in the $11e_1$ and $11e_3$ molecular orbitals which are essentially the plus and minus combinations of the $11e$ orbital of $Mn(CO)_5$, so that the result is practically nonbonding as far as the interaction between the two $Mn(CO)_5$ fragments is concerned. The only direct cross-interaction is found in the HOMO, which accounts for the metal–metal bond: this orbital has about 60% metallic

* To whom correspondence should be addressed.

0567-7408/82/010006-10$01.00

character, essentially $3d_{z^2}$ (27%) and $4p_z$ (24%), which establish a σ bond with the second metal. The $4p_z$ contribution enhances the density in the bond. However, there is also a 35% contribution of the π^* orbitals of the equatorial carbonyls which overlap (slightly) with the orbitals of both metals and tend to extend the density away from the bond axis. It should be noted that there is a good qualitative agreement between this HFS calculation and the extended CNDO calculation (Savariault, 1978), in particular for the HOMO. The essential difference is that the CNDO calculation gives less $4p$ and more $4s$ contribution. Savariault (1978) and Heijser *et al.* (1980) have both computed deformation-density maps which may be compared, at least at a qualitative level, with the result of an experimental determination.

It seemed of interest to look experimentally at the electron density in $Mn_2(CO)_{10}$ by accurate low-temperature X-ray diffraction measurements, even if the metal–metal bonding is not expected to give large features in the deformation-density maps. The study of $Mn_2(CO)_{10}$ was suggested by a previous work on $[Cp_2Fe(CO)_2]_2$ (Mitschler, Rees & Lehmann, 1978), another compound with a single metal–metal bond, in which no evidence was found for an accumulation of charge density on the metal–metal bond axis. But in that compound the bond is supported by two carbonyl bridges, and an *ab initio* calculation performed later by Bénard (1978) showed that the bonding was entirely due to a superexchange mechanism involving the π^* orbitals of the bridging carbonyls. Also of interest is the comparison with another metal carbonyl, $Cr(CO)_6$ (Rees & Mitschler, 1976), principally considering that in the present compound there are two chemically different types of carbonyl ligands.

Experimental

Well-formed single crystals of $Mn_2(CO)_{10}$ were obtained by sublimation of commercial material under vacuum at a temperature of 298 K, in about a week. The crystal used for the diffraction measurements was shaped into a sphere. We did not notice the instability under X-ray irradiation mentioned by Dahl & Rundle (1963). As these authors state, such an instability is probably due to impurities, such as water, which were not present in our crystal. The crystal was maintained at a temperature of 74 K by circulation of liquid nitrogen (under reduced pressure) in a beryllium cryostat secured in the χ circle of a Picker diffractometer. No phase change was noticed while the crystal was cooled.

The crystallographic characteristics are reported in Table 1. Following Dahl & Rundle (1963), and for easier comparison with the room-temperature results, we have chosen the space group $I2/a$, rather than the conventional group $C2/c$. The cell dimensions were determined through a least-squares procedure using the setting angles of 11 reflexions with $0{\cdot}6 < \sin\theta/\lambda < 0{\cdot}8$ Å^{-1} (Ag $K\alpha_1$ radiation). The setting angles taken for a given reflection hkl were the averages of those obtained by centring hkl at the counter position 2θ and $\bar{h}\bar{k}\bar{l}$ at position -2θ.

Two data sets have been collected, with the same crystal but two different X-ray wavelengths, Ag $K\alpha$ and Mo $K\alpha$. The conditions of data collection are summarized in Table 2. Three crystallographically equivalent sets of reflections have been measured with Ag $K\alpha$, up to a maximum angle of 2θ of 95°. However, for $2\theta > 65°$, only the most significant reflections were measured. For this purpose, a first estimate of intensity and background was made through a high-speed measurement, and only those reflections with a signal/noise ratio larger than a given threshold (variance from counting statistics less than about ten times the integrated intensity) were measured in the regular way. 30% of the reflections were thus effectively measured in the range 65 to 90°. This rate dropped to less than 2% for angles 2θ larger than 90°. The strongest reflections were measured with attenuators. The attenuation

Table 1. *Crystallographic characteristics*

Space group $I2/a$, $Z = 4$

Cell dimensions	74 K	RT*
a	14·088 (3) Å	14·16 (2) Å
b	6·850 (2) Å	7·11 (2) Å
c	14·242 (3) Å	14·67 (2) Å
β	105·08 (1)°	105·0 (5)°
V	1327·1 Å^3	1426·6 Å^3

* Room temperature: Dahl & Rundle (1963).

Table 2. *Data collection*

	I	II
Crystal diameter	0·225 ± 0·010 mm	
X-radiation	Ag $K\alpha$	Mo $K\alpha$
λ ($K\alpha_1$)	0·5594 Å	0·7093 Å
Linear absorption coefficient	0·968 mm^{-1}	1·878 mm^{-1}
Transmission factor	0·850–0·852	0·835–0·839
Temperature	74 ± 0·5 K	74 ± 0·5 K
Monochromator (graphite) 2θ	9·63°	12·17°
Type of measurement	Continuous scan $\theta/2\theta$	Flying step scan $\theta/2\theta$ Time interval: 2s
Total 2θ scan (without $\alpha_1\alpha_2$ splitting)	3·4°	3·4°
Speed in 2θ	2° min^{-1}	2° min^{-1}
Time of background measurement at each end of scan interval	20 s	Optimized
Max ($\sin\theta/\lambda$)	1·32 Å^{-1}	0·76 Å^{-1}
Number of reflections:		
measured	20478	2524
independent	7329	2411

factors, extrapolated to zero absorption, were determined, together with the counter dead-time constant, by the method described by Chipman (1969). The low-order reflections ($\sin\theta/\lambda < 0.76$ Å^{-1}), of particular importance because most charge-density maps were based on them, were measured again with Mo $K\alpha$ radiation. These measurements were done by the 'flying step-scan' technique: crystal and counter rotate in uniform $\theta/2\theta$ motion, but the counts are read at regular time intervals. A first estimate of intensity and background was done as described above, but it was used here to optimize the time of the background measurements, at each end of the scanning interval, so that the times spent on the peak and on the background are roughly proportional to the square root of the respective intensities (Shoemaker, 1968). No attenuators were used during this series of measurements, but the strongest reflections were measured again at reduced X-ray-tube intensity. To integrate the diffracted intensities we used a local version of the program *PROFIL* (Blessing, Coppens & Becker, 1974), based on the method developed by Lehmann & Larsen (1974). Dead-time corrections were applied to the strong reflections.

Each data set was corrected as usual and averaged over the crystallographically equivalent reflections. [Agreement index for the Ag $K\alpha$ set: 0·023 ($\sin\theta/\lambda < 0.76$ Å^{-1}), 0·171 ($\sin\theta/\lambda > 0.76$ Å^{-1}).] Least-squares refinements were performed, using the free-atom form factors and anomalous-dispersion factors of *International Tables for X-ray Crystallography* (1974).

A conventional refinement of all Ag $K\alpha$ data such that $I > 3\sigma(I)$ (4583 reflections) gave the following figures of merit: $R(F) = 0.047$, $R_w(F) = 0.030$, goodness-of-fit (g.o.f.) = 1·58. The extinction was found to be negligible. Final atomic positional and thermal parameters, reported in Tables 3 and 4, were obtained in a high-order refinement, in which all measured Ag $K\alpha$ data such that $\sin\theta/\lambda > 0.76$ Å^{-1} were included [$R(F) = 0.144$, $R_w(F) = 0.070$, g.o.f. = 1·10]. In this calculation, the scale factor was fixed at the value obtained in the conventional refinement.

The final values taken for the low-order structure factors were weighted averages of the dispersion-corrected structure factors observed with the two radiations. They were scaled to the structure factors calculated in the spherical free-atom approximation, with the atomic parameters determined as above.*

Molecular geometry

The numbering of the atoms is shown in Fig. 1. The observed bond lengths and bond angles are reported in Tables 5 and 6. The bond lengths were corrected for the apparent shortening due to thermal librations, assuming a riding motion of each carbonyl group, as a whole, around Mn. This assumption is supported by the observation that the amplitude of angular motion around Mn is nearly always the same for C and O of the same carbonyl (Table 7). The motion of the axial carbonyls is larger than that of the equatorial carbonyls, probably because the steric hindrance is less. Also shown in Table 7 are the extra amplitudes of motion of the carbonyls, relative to Mn, along the bond

* A list of structure factors has been deposited with the British Library Lending Division as Supplementary Publication No. SUP 36321 (31 pp.). Copies may be obtained through The Executive Secretary, International Union of Crystallography, 5 Abbey Square, Chester CH1 2HU, England.

Table 3. *Atomic positions* ($\times 10^5$) *from high-angle X-ray data and mean isotropic B values* (Å^2)

	x	y	z	B
Mn	34564 (2)	23692 (4)	6916 (2)	0·831 (2)
C(1)	46079 (13)	24566 (36)	16297 (15)	1·552 (20)
O(1)	53217 (18)	25179 (65)	22392 (23)	2·629 (45)
C(2)	39308 (12)	34614 (26)	−2901 (15)	1·144 (16)
O(2)	42255 (14)	40734 (31)	−8989 (15)	1·577 (18)
C(3)	27735 (15)	11888 (27)	14897 (13)	1·200 (16)
O(3)	23749 (19)	4557 (30)	19958 (16)	1·714 (21)
C(4)	37361 (13)	−425 (30)	2469 (15)	1·166 (17)
O(4)	39594 (15)	−14933 (29)	−285 (19)	1·698 (20)
C(5)	30906 (13)	48440 (26)	10161 (12)	1·072 (15)
O(5)	28840 (14)	63707 (24)	12104 (12)	1·363 (16)

Table 4. *Thermal parameters* (Å^2 × 10^4) *from high-angle X-ray data*

The temperature factor is $\exp(-2\pi^2 \sum_i \sum_j h_i a_i^* h_j a_j^* U_{ij})$.

	U_{11}	U_{22}	U_{33}	U_{12}	U_{13}	U_{23}
Mn	92·0 (4)	103·6 (6)	113·4 (5)	−1·1 (8)	14·5 (4)	22·1 (8)
C(1)	146 (4)	211 (7)	195 (5)	−14 (5)	−22 (4)	57 (6)
O(1)	211 (6)	406 (13)	286 (9)	−36 (9)	−107 (6)	105 (11)
C(2)	120 (4)	160 (5)	158 (5)	−6 (3)	43 (4)	38 (4)
O(2)	186 (5)	226 (6)	207 (6)	−16 (4)	86 (4)	61 (5)
C(3)	194 (5)	140 (5)	130 (5)	−10 (4)	57 (4)	6 (4)
O(3)	321 (8)	195 (5)	174 (5)	−53 (5)	134 (5)	4 (4)
C(4)	135 (4)	126 (5)	191 (6)	18 (4)	59 (4)	25 (4)
O(4)	211 (5)	151 (5)	301 (8)	47 (4)	97 (5)	4 (5)
C(5)	151 (4)	122 (5)	122 (4)	−26 (4)	15 (3)	3 (4)
O(5)	230 (5)	117 (4)	156 (4)	−11 (4)	24 (4)	14 (3)

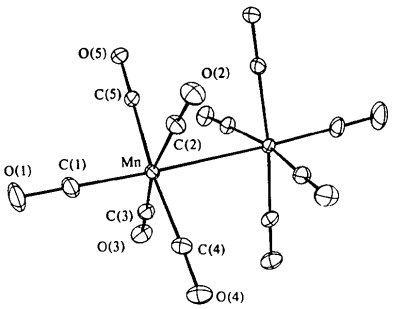

Fig. 1. $Mn_2(CO)_{10}$ in the crystal at 74 K. Thermal ellipsoids include regions of 50% probability.

Table 5. *Interatomic distances* (Å)

	Uncorrected	Corrected		Uncorrected	Corrected
Mn–Mn′	2·8950 (6)	2·895 (1)	C(1)–O(1)	1·146 (3)	1·150 (4)
			C(2)–O(2)	1·134 (3)	1·136 (4)
Mn–C(1)	1·815 (2)	1·820 (3)	C(3)–O(3)	1·139 (3)	1·140 (4)
Mn–C(2)	1·857 (2)	1·860 (3)	C(4)–O(4)	1·142 (3)	1·144 (4)
Mn–C(3)	1·855 (2)	1·858 (3)	C(5)–O(5)	1·139 (3)	1·141 (4)
Mn–C(4)	1·848 (2)	1·850 (3)			
Mn–C(5)	1·865 (2)	1·867 (3)			

Table 6. *Bond angles* (°)

C(1)–Mn–Mn′	175·33 (6)	C(2)–Mn–C(3)	169·36 (8)
C(2)–Mn–Mn′	86·63 (4)	C(4)–Mn–C(5)	174·24 (8)
C(3)–Mn–Mn′	82·97 (4)	C(2)–Mn–C(4)	87·23 (8)
C(4)–Mn–Mn′	90·60 (4)	C(2)–Mn–C(5)	89·84 (8)
C(5)–Mn–Mn′	84·28 (4)	C(3)–Mn–C(4)	90·64 (8)
		C(3)–Mn–C(5)	91·35 (8)
C(1)–Mn–C(2)	96·50 (9)		
C(1)–Mn–C(3)	94·01 (9)	Mn–C(1)–O(1)	178·27 (26)
C(1)–Mn–C(4)	93·00 (10)	Mn–C(2)–O(2)	177·93 (20)
C(1)–Mn–C(5)	92·25 (10)	Mn–C(3)–O(3)	178·36 (21)
		Mn–C(4)–O(4)	176·17 (17)
		Mn–C(5)–O(5)	178·60 (17)

Table 7. *Thermal motion of the carbonyls*

	Perpendicular to the bond Amplitude of angular motion (°)		Parallel to the bond Amplitude of linear motion (Å)	
	C	O	C	O
C(1)–O(1)	4·99 (8)	4·99 (7)	0·049 (4)	0·042 (5)
C(2)–O(2)	3·21 (8)	3·12 (4)	0·033 (8)	0·041 (6)
C(3)–O(3)	3·29 (9)	3·42 (5)	0·051 (5)	0·040 (6)
C(4)–O(4)	3·28 (9)	3·37 (4)	0·040 (7)	0·041 (6)
C(5)–O(5)	2·42 (11)	2·62 (4)	0·054 (5)	0·037 (6)

Amplitude of angular motion: $\left(\frac{U_A - U_{Mn}}{MnA}\right)^{1/2} \times \frac{180}{\pi}$

(U's in the plane perpendicular to the bond).

Amplitude of linear motion: $(U_A - U_{Mn})^{1/2}$

(U's in the direction of the bond).

direction. This motion is the main reason for the failure of a rigid-body model to fit the data.

The bond lengths are in good agreement with the values obtained by electron diffraction in the gas phase (Almenningen *et al.*, 1969), and by X-rays at room temperature (Dahl & Rundle, 1963). The Mn–Mn bond is the striking exception. This bond is already significantly shorter in the crystal at room temperature than in the gas [2·923 (3) *vs* 2·977 (11) Å]; it becomes even shorter at low temperature [2·895 (1) Å]. Such behaviour is obviously related to the low bond-dissociation energy [between 42 and 155·4 kJ mol^{-1}, depending on whether or not relaxation of the $Mn(CO)_5$ radicals is allowed for, see Haines, Hopgood & Poë (1968)]. The shortening of the Mn–Mn bond in the crystal upon cooling is probably due not only to larger intermolecular interactions at low temperature (shown by the reduction in the cell dimensions) which would tend to compress the molecule, but also to a depopulation of excited Mn–Mn vibrational levels, as shown by the large energy increase (500 cm^{-1}) of the $\sigma \rightarrow \sigma^*$ band of the electronic spectrum in solution (Levenson & Gray, 1975).†

The axial Mn–C bonds are shorter than the equatorial bonds, in agreement with the two other experimental studies. The experimental accuracy here is also sufficient to distinguish between longer axial C–O bonds (1·150 Å), and shorter equatorial C–O bonds which range from 1·136 to 1·144 Å, with an average value of 1·140 Å. Such differences imply a stronger bonding of the axial carbonyls, which will be further discussed below. They are in agreement with the force constants reported by Bor & Sbrignadello (1974): $16{\cdot}308 \times 10^{-8}$ and $16{\cdot}500 \times 10^{-8}$ N $Å^{-1}$, for axial and equatorial CO respectively.

There are significant differences between the four equatorial Mn–C bonds, which seem to be sensitive to intermolecular interactions, in contrast to C–O bonds. This is not surprising when the force constants are compared: about 2×10^{-8} N $Å^{-1}$ for a metal–carbon bond, and 17×10^{-8} N $Å^{-1}$ for a CO bond (Jones, McDowell & Goldblatt, 1969).

The flexibility of the molecule becomes more apparent with the bond angles (Table 6). Comparison with the room-temperature results (Dahl & Rundle, 1963) shows that the distortion is qualitatively the same at both temperatures. It is best analysed by considering spherical coordinates, with the origin at Mn, as expressed in Table 8. The axes were defined for an undistorted $Mn(CO)_5$ fragment with $C_{ax}MnC_{eq} = 93{\cdot}4°$ (Almenningen *et al.*, 1969): Z along $Mn–CO_{ax}$,

† *Note added in proof:* the room-temperature crystal structure of $Mn_2(CO)_{10}$ has been redetermined recently (Churchill, Amoh & Wassermann, 1981). The Mn–Mn distance, 2·9038 (6) Å, is considerably shorter than in the earlier determination, but the shortening at reduced temperature remains significant.

Table 8. *Spherical coordinates*

	r (Å)	θ (°)	φ (°)
Mn	0	—	—
C(1)	1·815 (2)	0·82 (8)	164 (5)
O(1)	2·960 (2)	1·48 (8)	157 (3)
C(2)	1·857 (2)	95·71 (5)	−1·06 (6)
O(2)	2·991 (2)	95·76 (4)	−1·85 (4)
C(3)	1·855 (2)	94·80 (6)	−179·41 (6)
O(3)	2·994 (2)	94·19 (5)	−179·29 (4)
C(4)	1·848 (2)	92·76 (6)	−88·54 (6)
O(4)	2·989 (2)	91·78 (5)	−87·46 (4)
C(5)	1·865 (2)	92·46 (5)	89·02 (5)
O(5)	3·003 (2)	92·18 (3)	88·57 (4)
Mn′	2·895 (1)	175·99 (1)	124·49 (8)
b axis	—	87·97	64·81

Table 9. *Angular distortion of the molecule* (°)

	Free molecule	R.m.s. distortion[a] 74 K	RT	Force constant ($\times 10^{-8}$ N Å^{-1})
C_{eq}–Mn–C_{eq}	90	1·57	1·0	0·57[c]
C_{ax}–Mn–C_{eq}	93·4 (5)[b]	1·60	1·2	0·34[c]
Mn′–Mn–C_{eq}	86·6 (5)[b]	2·90	1·7	0·10[c]
Mn–C–O	180	2·30	2·6	0·5[d]
Molecular torsion	45	5·67	2·6	0·1

(*a*) Defined in the text. (*b*) By electron diffraction in the gas phase (Almennigen *et al.*, 1969). (*c*) Quicksall & Spiro (1969). (*d*) Jones *et al.* (1969).

X and Y in two perpendicular $C_{ax}MnC_{eq}$ planes. The coordinates of Table 8 were obtained by superposing the actual $Mn(CO)_5$ fragment on the idealized one, so as to minimize the distances between the corresponding nuclei by a least-squares procedure (locally written program *COMPAR*).

In this new axial frame e.s.d.'s of the Cartesian coordinates X (and hence of the spherical coordinates) were computed from the equation $\mathbf{C}_X = \tilde{\mathbf{T}}^{-1}\,\mathbf{C}_x\,\mathbf{T}^{-1}$, where $\mathbf{C}_X$ and $\mathbf{C}_x$ are the variance-covariance matrix in the new frame and in the crystal axes respectively, $\mathbf{T}$ the transformation matrix [$\mathbf{X} = \mathbf{T}(\mathbf{x} - \mathbf{x}_{Mn})$] and $\tilde{\mathbf{T}}$ its transpose.

The strongest distortions concern the relative position of the two $Mn(CO)_5$ groups of the molecule, as shown by the coordinates of the second Mn atom (MnMn′ is 4° off the z axis) and by the orientation of the b axis, which is parallel to the molecular symmetry axis: from the value of 64·8°, the torsional angle around the molecular axis is 50·4°. At room temperature this angle is 47·4°, much closer to the value of an ideally staggered conformation (45°). The angle θ of 88·0° implies a bending of 4° of the whole molecule.

We may define a r.m.s. distortion of a structural quantity α, with unstrained value α_o and n values α_i in the crystal, as: $D(\alpha) = |\sum_i (\alpha_i - \alpha_o)^2/n|^{1/2}$. If α_i and α_o are observed values, with e.s.d.'s $\sigma(\alpha_i)$ and $\sigma(\alpha_o)$, an unbiased estimate of D is provided by:

$$D(\alpha) = \left\{ \sum_i |(\alpha_i - \alpha_o)^2 - \sigma^2(\alpha_i)|/n - \sigma^2(\alpha_o) \right\}^{1/2}.$$

Values of $D(\alpha)$, calculated at low and room temperature, are reported in Table 9. The molecule is clearly more distorted at low temperature, due to closer intermolecular contacts and thus stronger interactions. The force constants have also been indicated in the table. They come essentially from the normal-coordinate analysis of Quicksall & Spiro (1969). The force constant for molecular torsion is only a rough estimate, assuming a barrier for rotation of 8·4 kJ mol^{-1} (Almenningen *et al.*, 1969) and a sinusoidal variation of energy with the torsion angle.

There is a clear inverse correlation between the average distortion and the force constant. The r.m.s. distortion of the Mn–C–O angle is somewhat large considering the assumed force constant, which could be wrong because it had not been refined for $Mn_2(CO)_{10}$ and was taken from the normal-coordinate analysis of $Cr(CO)_6$ (Jones *et al.*, 1969). But more probably the r.m.s. distortion is overestimated, due to our assumption of an unconstrained Mn–C_{eq}–O_{eq} angle of 180°. In fact it is seen in Table 8 that all equatorial O atoms but one are bent away from Mn′, the average component of the Mn–C–O angle in the Mn′MnCO plane being 178·8°. By refining this angle from their electron diffraction data, Almenningen *et al.* (1969) had found an angle of 178·6°, but in the opposite direction.

Electron-density distribution

The X–X deformation density (total density *minus* free spherical atoms) was computed as follows: the positional and thermal parameters of the spherical atoms were those of Tables 3 and 4 (from the refinement of Ag $K\alpha$ reflections with $\sin\theta/\lambda > 0{\cdot}76$ Å^{-1}). The total density was obtained by taking all observed reflections to a maximum $\sin\theta/\lambda$ value of 0·76 Å^{-1}. Unless explicitly stated otherwise the deformation densities discussed hereafter are those of this resolution. The scale factor was determined by scaling the observed and the calculated density in one refinement cycle.

This procedure was first applied to the Ag $K\alpha$ data only. At the mid-point of the Mn–Mn bond a slightly positive (0·10 e Å^{-3}) deformation density was obtained, with an e.s.d. (Rees, 1978) of 0·10 e Å^{-3}, this rather large value being due to the presence of the crystallographic symmetry axis. The observed residual density is thus not significant. This ambiguity prompted us to collect a second data set with Mo $K\alpha$ radiation, and the structure factors of both sets were finally averaged, as described above.

Determination of atomic charges

Atomic charges were determined both in real space by direct integration, and in reciprocal space by least-squares refinement. In the first case, the integration volumes around the atoms were defined either as adjacent polyhedra, or as intersecting spheres. In each case their size was determined by integration of the calculated density: since the atoms are neutral in the free-atom model, this integration must yield the atomic numbers. For this volume definition, series-termination effects are important and must be corrected for, especially in the spherical case: if this correction is not done the integrated charge oscillates as the radius of the sphere is increased. In the case of polyhedra, this effect is much smaller. Nevertheless the size of the polyhedra was defined from the highest resolution of our experiment. On the other hand, the integration of $F_o - F_c$ to determine the net charges does not suffer from series termination: the results obtained with the full data set and those from the low-order data alone never differed by more than a fraction of the e.s.d. The results from the low-order data are given in Table 10. The polyhedra considered were square prisms of $2{\cdot}1 \times 2{\cdot}1$ Å^2 section, directed along the bond axes. (The value of 2·1 Å was obtained by imposing the equidistance of Mn to five of the six planes of its integration volume, the sixth one bisecting the Mn–Mn bond.) Details on the method of integration and the estimation of the standard deviations will be given elsewhere (Rees & Wiest, 1981).

It must be noted that neither of the two definitions of atomic volumes achieves a complete partition of space (Coppens, Moss & Hansen, 1980). We feel, however, that since only regions distant from the atomic centres are left out, their inclusion would not essentially change the results. More questionable is the use of overlapping volumes, as in the spherical integration, for in this case part of the charge is obviously counted twice. The largest bias occurs for strongly bonded atoms, both because of the large overlap in the bonding region (due to the shortness of the bond), and the large residual charge in this region. An excessive negative charge is therefore found for such atoms, and the results quoted in Table 10 (third column) show this to be so in the present analysis for the C and O atoms. There is much less bias for Mn, the charge of which is probably intrinsically negative. The charges may be tentatively normalized along these lines by adding a common quantity to all C and O charges so that the molecule becomes neutral (fourth column of Table 10).

The polyhedral model confirms the negative charge of Mn. The separation between carbon and oxygen is rather unsatisfactory, the O atoms being more positively charged than the C atoms. This is perhaps not too surprising, considering the large covalency of the CO bonds. But the two direct integration methods agree on one important feature: the axial carbon has a larger electron population than the equatorial carbons.

It must also be emphasized that the charges found with both methods are very small, so that all atoms,

Table 10. *Atomic charges (in electrons)*

	Integration in real space					κ-refinement			
	Intersecting spheres			Square prisms (2·1 × 2·1 Å^2)		Valence shell $3d^m$		Valence shell $3d^m4s^p$	
	Radius (Å)	Charge	Normalized charge[a]	Length (Å)	Charge	κ	Charge	κ	Charge
Mn	1·28	−0·16 (8)	−0·16	2·51	−0·08 (9)		+0·92 (5)		−0·59 (15)
3*d* population						0·958 (5)	6·08 (5)	1·066 (10)	5·25 (10)
4*s* population							0	1·326 (31)	2·34 (13)
C(1)	0·98	−0·16 (3)	+0·01	1·50	−0·08 (5)	1·017 (5)	−0·35 (6)	1·057 (5)	−0·14 (6)
C(2)	0·97	−0·11 (3)	+0·06	1·58	+0·01 (5)	1·055 (3)	+0·10 (4)	1·107 (4)	+0·39 (5)
C(3)	0·97	−0·13 (3)	+0·04				+0·01 (4)		+0·31 (5)
C(4)	0·97	−0·11 (3)	+0·06	1·59	+0·02 (5)		−0·06 (5)		+0·32 (5)
C(5)	0·97	−0·12 (3)	+0·05				−0·08 (5)		+0·25 (5)
O(1)	0·99	−0·12 (3)	+0·05	2·96	+0·02 (6)	1·042 (3)	+0·02 (5)	1·044 (3)	−0·06 (5)
O(2)	0·97	−0·22 (3)	−0·05	2·88	+0·08 (6)	0·995 (2)	−0·51 (4)	1·009 (2)	−0·50 (3)
O(3)	0·97	−0·26 (3)	−0·09				−0·55 (4)		−0·51 (3)
O(4)	0·97	−0·18 (3)	−0·01	3·09	+0·10 (6)		−0·46 (4)		−0·45 (3)
O(5)	0·97	−0·15 (3)	+0·02				−0·40 (4)		−0·40 (3)
Scale factor						0·988 (2)		0·976 (2)	
ΔQ^b						0·39		5·02	
$R(F)$						0·032		0·031	
$R_w(F)$						0·027		0·025	
g.o.f.						2·69		2·50	

(*a*) See text. (*b*) Sum of charges without constraints.

including the metal, in this Mn^0 complex, are almost neutral.

The κ-refinement method was used to determine the charges in reciprocal space (Coppens, Guru Row, Leung, Stevens, Becker & Yang, 1979). The core scattering factor of Mn was obtained by subtracting a $3d^5 4s^2$ valence shell from the relativistic Hartree–Fock factor of Mn. The scattering factor of the Mn atom and that of its $3d$ shell were taken from *International Tables for X-ray Crystallography* (1974). The $4s$ scattering factor was computed by Cromer (1977, unpublished work).

The valence shell of Mn was first assumed to be of $3d$ type only, then as a combination of $3d$ and $4s$. The results of both calculations are reported in Table 10. ΔQ is the change which would occur in the total number of electrons of the asymmetric unit if no charge constraint was applied [the total charge of the molecule is constrained to remain invariant by the method described by Hamilton (1964)]. Constraint is also placed on the contraction coefficients κ of the equatorial carbonyls (carbon and oxygen). These refinements were made with the low-order data, all positional and thermal parameters being fixed at the values obtained in the high-order refinement (Tables 3 and 4).

This method gives larger charges on the atoms than does integration in direct space. The charge of Mn, however, is hardly defined at all, because the occupancy of the fourth shell is very inaccurate. This is due to the diffuseness of the electron density in this shell: the $4s$ scattering factor (Cromer, 1977, unpublished work) falls so rapidly that it is zero for $\sin\theta/\lambda = 0{\cdot}19$ Å^{-1}; the sphere defined by this value contains only 38 independent reflections! However, the large κ coefficient indicates that this shell is contracted in the complex. Comparing with the results obtained with a pure $3d$ valence shell, it is seen that, when $4s$ electrons are allowed in the calculation, both the positive charge and the contraction of the C atoms increase, while the oxygen parameters are much less affected. This shows that part of the electrons between Mn and the carbonyls is attributed either to the C atoms or to the fourth shell of Mn. The improvement of the residuals due to consideration of $4s$ electrons is statistically significant, but the large charge excess ΔQ must be noted. The scale factor is highly correlated with the κ coefficient of Mn $3d$ (correlation coefficient: $-0{\cdot}9$), and this may explain its rather large change when compared with the free-atom model [scale factor = 0·998, $R(f) = 0{\cdot}034$, $R_w = 0{\cdot}031$, g.o.f. = 3·05].

Again, the difference between axial and equatorial carbonyls is striking. There is even an inversion of polarity in the axial carbonyl, where carbon is more negatively charged than oxygen. This may indicate a large occupancy of the π^* orbitals of CO, which more than compensates the electron loss of carbon due to the σ-bond with the metal: the π^* orbitals are more concentrated on carbon, as shown by the Mulliken populations, which are reversed relative to the π orbitals [1·38 e on carbon, 0·62 e on oxygen, taking for example the calculation of Ransil (1960)].

Deformation density in the M–M bond region

The chemically averaged deformation density is shown in Fig. 2.

Before averaging, and because of the geometrical distortions of the molecule, care had to be taken that the density was calculated at chemically equivalent points. To do this properly bond axes were chosen as local axes: O(1)Mn, MnMn′ or Mn′O(1)′ were taken as the x axis, and the considered equatorial MnO bond for the y axis.

This deformation-density map, although more accurate than the maps calculated with the Ag $K\alpha$ data alone, does not differ essentially from them. The deformation density at the mid-point of the Mn–Mn bond is still positive (0·05 e Å^{-3}), and still not significant (e.s.d. = 0·07 e Å^{-3}). A closer examination shows that the slightly positive deformation density extends very far into the plane perpendicular to the Mn–Mn bond, at its mid-point. By integration over all points closer than 0·2 Å to this plane, and within 1·5 Å from the Mn–Mn axis, a total excess of 0·037 electron is obtained, with an e.s.d. of 0·022 electron. Apart from the small peak on the metal–metal bond, second maxima of 0·05 e Å^{-3} are observed away from the bond, approximately between Mn′ and the equatorial C atoms bonded to the other Mn atom. Although the accuracy of the average deformation density is better in this region, away from the symmetry axis and from the molecular axis (e.s.d. = 0·035 e Å^{-3}), the observed features are too small, so they cannot be considered as a proof of direct interaction between the equatorial carbonyls and the other manganese (Brown *et al.*, 1971). On the other hand the fact that only a very small deformation density is observed between the metal atoms is supported by the theoretical results of Heijser

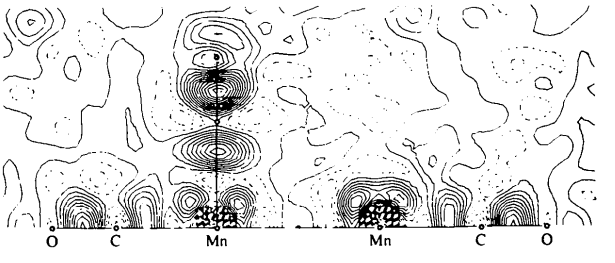

Fig. 2. Average deformation density. Resolution: $\sin\theta/\lambda <$ 0·76 Å^{-1}. Contour interval: 0·05 e Å^{-3}. Negative contours are dashed. The average e.s.d. of ρ_{obs}, in a general position, is 0·07 e Å^{-3} before averaging, 0·03 e Å^{-3} after averaging (except for points within 0·4 Å of the molecular axis).

et al. (1980) in the Hartree–Fock–Slater approximation. There is indeed a remarkable qualitative agreement between their Hartree–Fock–Slater deformation density and our experimental result. Thermal motion and limited experimental resolution may account for most of the quantitative differences between our deformation-density maps and Fig. 4(*b*) of Heijser *et al.* (1980), namely the elongation of the carbonyl peaks normal to the CO direction, the reduction in height of the peaks around the metal and their displacement away from the centre of the atom, in the experimental map (see also below).

Metal configuration

Fig. 2 shows clearly that the metal configuration is octahedral to a good approximation: minima of −0·1 to −0·2 e Å^{-3} in the deformation density are seen on the bond axes at about 0·8 Å from the metal nucleus, and maxima of 0·3 to 0·4 e Å^{-3} on the body diagonals, at about 0·6 Å. There is no evidence for a participation of $4p_z$ in the Mn–Mn bonding as found in the calculation of Heijser *et al.* (1980): this would result in a lower density in the Mn–C_{ax} direction than in the Mn–Mn′ direction, while actually the opposite is observed (the difference being however statistically insignificant). But two phenomena concur to render the $4p_z$ participation, if any, unobservable: the first is the diffuseness of $4p$ orbitals. The second is that thermal motion and limited resolution push the features of the deformation density away from the Mn nucleus (see below): the minimum on the C_{ax} side approaches the region of the carbonyl σ lone pair, which tends to cancel it. Indeed a trend to correct this situation is observed at higher resolution: when all observed intensities up to $\sin\theta/\lambda = 0{\cdot}95$ Å^{-1} are included in the density calculation, the depths of the two minima become almost equal (0·28 and 0·35 e Å^{-3} on the C_{ax} and on the Mn side, respectively, compared to 0·10 and 0·23 e Å^{-3} at 0·76 Å^{-1}).

The minima on the molecular axis do not significantly differ from those in the Mn–C_{eq} directions: this suggests that the occupancies of $3d_{z^2}$ and $3d_{x^2-y^2}$ orbitals are not very different. On the other hand the density is slightly less in the [110] direction of the octahedron (the normal to the molecular axis at Mn′ in Fig. 2) than in the [011] and [101] directions (the bond bisectors at Mn), the difference, 0·08 e Å^{-3}, being a little less than 2σ. The order of occupancy of the $3d$ orbitals is therefore:

$$z^2 \simeq x^2 - y^2 < xy < xz = yz.$$

Although the molecular symmetry is not octahedral, there are still clearly two groups of d orbitals: z^2 and x^2-y^2 on one hand (the e_g orbitals in an octahedral environment), xy, yz and xz (the 't_{2g}' orbitals) on the other. From the observed density, it is possible to determine the difference of the average occupancy of the two groups, in the way used in the study of $Cr(CO)_6$ (Rees & Mitschler, 1976).

Assuming a cubic environment of the metal and writing its valence-shell configuration as $(3d_{t2g})^{3m}(3d_{eg})^{2n}(4s)^p$, it can be shown that the difference in deformation densities $\Delta\rho_{111} - \Delta\rho_{100}$ is proportional to $(m-n)$. The proportionality coefficient may be determined by calculating the Fourier transform of the aspherical part of the $3d$ scattering factor, thermally averaged and at the same resolution. The total number of valence electrons was assumed to be seven, as direct integration had shown that the charge of Mn was very small. The calculation was done for the two configurations $3d^54s^2$ (*International Tables for X-ray Crystallography*, 1974) and $3d^7$ (Watson & Freeman, 1961). The proportionality coefficients, obtained by fitting the theoretical and experimental curves up to 0·6 Å from the Mn nucleus, were 2·0 (2) and 2·3 (2) respectively. From those values, 24 (2)% of the d electrons occupy the 'e_g' orbitals in a $3d^54s^2$ configuration and 27 (2)% in a $3d^7$ configuration. Quite similar results had been obtained for Cr in $Cr(CO)_6$, where the proportion of e_g electrons was 25%.

Fig. 3 shows $\Delta\rho_{111} - \Delta\rho_{100}$ together with the scaled theoretical curves for the two configurations. $\Delta\rho_{111}$ is the deformation density averaged over the eight directions of the body diagonals. $\Delta\rho_{100}$ is the average over the four equatorial Mn–CO directions. The error bars represent $\pm\sigma$. For the calculation of the e.s.d., an estimate of the covariance between $\Delta\rho$ in the various directions is required (Rees, 1976). Both the experimental and the theoretical curves have been calculated for 2θ cut-off values of 0·76, 0·95 and 1·32 Å^{-1} (the whole data set). The scaling coefficient applied to all theoretical curves was that determined from the low-order data set (2·0 or 2·3). As expected, the height of both the experimental and the theoretical peaks increases, while its position is shifted toward the nucleus, as the resolution is improved.

The carbonyls

Of further interest is the charge density in the carbonyl regions. Since the density is essentially cylindrically symmetric, the cylindrical average of the deformation density around each CO bond direction was calculated (Rees & Wiest, 1981), and, in the case of the equatorial bonds, the result was averaged over the four independent bonds. The result may be compared to the theoretical density of carbon monoxide, as it would appear under the same conditions of thermal motion and limited resolution. The wave function of CO was that of McLean & Yoshimine (1967). Details of such a calculation were given by Rees & Mitschler (1976).

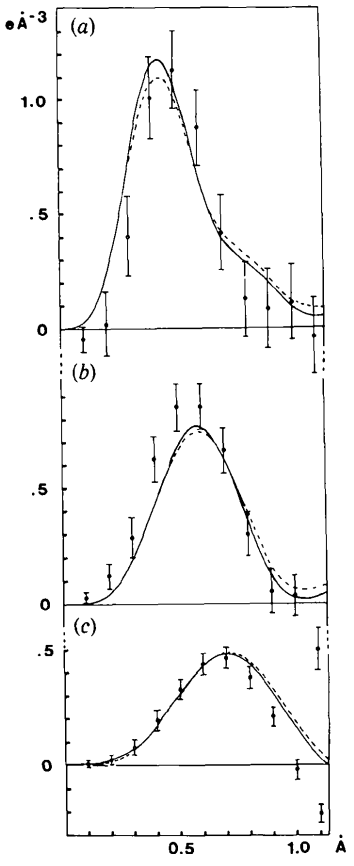

Fig. 3. $\Delta\rho_{111} - \Delta\rho_{100}$ around a Mn centre, at three resolutions: (*a*) $\sin\theta/\lambda < 0{\cdot}76$ Å^{-1}; (*b*) $\sin\theta/\lambda < 0{\cdot}95$ Å^{-1}; (*c*) $\sin\theta/\lambda < 1{\cdot}32$ Å^{-1}. Points with error bars represent experimental average values plus or minus one e.s.d. The solid curves are calculated values for a $3d^5 4s^2$ configuration, with a scale factor of 2·0 (see text). The dashed curves are calculated for a $3d^7$ configuration with a scale factor of 2·3.

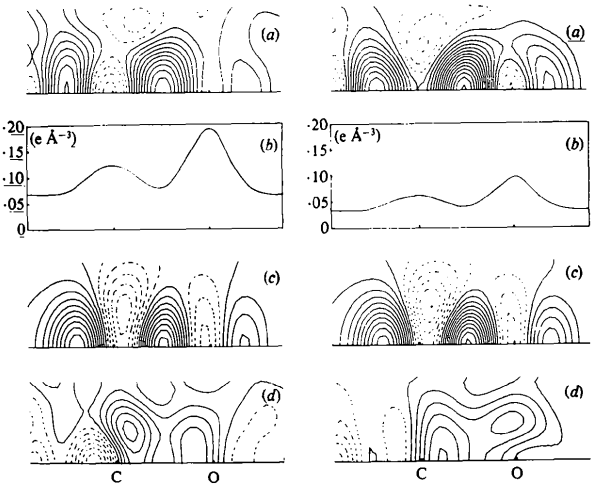

Fig. 4. Axial carbonyl (left) and average equatorial carbonyl (right). (*a*) Observed deformation density (cylindrical average); (*b*) e.s.d. of the deformation density along C–O axis; (*c*) calculated for carbon monoxide; (*d*) difference (*a*)–(*c*).

Fig. 4 shows both observed and theoretical densities, and their difference, for the axial and equatorial carbonyls. In both cases the difference maps display an electron deficiency in the region of the carbon lone pair, and two electron accumulations in the region of the atoms, with maxima which are either off the bond axis, or very elongated in the perpendicular plane. Similar features were encountered in chromium hexacarbonyl (Rees & Mitschler, 1976) and may be interpreted in terms of σ bonding and π back-donation: part of the electrons of the HOMO of carbon monoxide, which is essentially the carbon σ lone pair, are given to the metal, and this is more or less compensated by a partial occupation of the LUMO, the π^* orbitals. Moreover, the electron deficiency is significantly larger in the axial than in the equatorial carbonyls, which is consistent with a stronger bonding of the former. The reason for this is probably that CO ligands have a larger *trans* influence (Appleton, Clarck & Manzer, 1973) than the $Mn(CO)_5$ group. There is also a larger electron accumulation in the π region of the axial carbon. This becomes apparent if it is realized that the corresponding peak, though of the same magnitude as in the equatorial carbonyl, is about 0·4 Å off the bond axis, and thus integrates to a much larger value. The oxygen π peak is slightly smaller in the axial carbonyl but (*a*) as noted above, the π^* orbital is essentially localized on carbon and (*b*) the difference could be due to the larger thermal libration of the axial carbonyls.

To summarize, this study suggests that the formation of a long, single metal–metal bond as in $Mn_2(CO)_{10}$ has very little effect on the electron density of the separate fragments. Although there is some indication of a small charge-density accumulation in the plane perpendicular to the Mn–Mn bond through its midpoint, the present accuracy is not sufficient to distinguish this unambiguously from the statistical background, and *a fortiori* to decide whether or not there is a cross-interaction between one metal and the equatorial carbonyls bonded to the other metal atom. The electron configuration of each metal is practically octahedral. The configuration of the carbonyls is clearly different from uncomplexed carbon monoxide, and this difference is larger for the axial than for the equatorial carbonyls, a result in agreement both with the observed bond lengths and with the experimentally determined atomic charges. The good agreement between the experimental results reported here and the best available quantum chemical calculation (Heijser *et al.*, 1980) is noteworthy. The method of experimental charge-density determination used in this study is the only one capable of providing such a direct experimental support to elaborate quantum chemical calculations on medium-sized molecules.

References

ALMENNINGEN, A., JACOBSEN, G. G. & SEIP, H. M. (1969). *Acta Chem. Scand.* **23**, 685–686.

APPLETON, T. G., CLARCK, H. C. & MANZER, L. E. (1973). *Coord. Chem. Rev.* **10**, 335–422.

BAU, R., KIRTLEY, S. W., SORRELL, T. N. & WINARKO, S. (1974). *J. Am. Chem. Soc.* **96**, 988–993.

BÉNARD, M. (1978). *J. Am. Chem. Soc.* **100**, 7740–7742.

BLESSING, R. H., COPPENS, P. & BECKER, P. (1974). *J. Appl. Cryst.* **7**, 488–492.

BOR, G. & SBRIGNADELLO, G. (1974). *J. Chem. Soc. Dalton Trans.* pp. 440–448.

BROWN, D. A., CHAMBERS, W. J., FITZPATRICK, N. J. & RAWLINSON, R. M. (1971). *J. Chem. Soc. A*, pp. 720–725.

CHIPMAN, D. R. (1969). *Acta Cryst.* A**25**, 209–214.

CHURCHILL, M. R., AMOH, K. N. & WASSERMANN, H. J. (1981). *Inorg. Chem.* **20**, 1609–1611.

COPPENS, P., GURU ROW, T. N., LEUNG, P., STEVENS, E. D. BECKER, P. J. & YANG, Y. W. (1979). *Acta Cryst.* A**35**, 63–72.

COPPENS, P., MOSS, G. & HANSEN, N. K. (1980). *Computing in Crystallography*, edited by R. DIAMOND, S. RAMASESHAN & K. VENKATESAN, pp. 16.01–16.21. Bangalore: Indian Academy of Sciences.

DAHL, L. F. & RUNDLE, R. E. (1963). *Acta Cryst.* **16**, 419–426.

FREUND, H. J., DICK, B. & HOHLNEICHER, G. (1980). *Theor. Chim. Acta*, **57**, 181–207.

HAINES, L. I. B., HOPGOOD, D. & POË, A. J. (1968). *J. Chem. Soc. A*, pp. 421–428.

HAMILTON, W. C. (1964). *Statistics in Physical Science*, Section 4.5. New York: Ronald Press.

HEIJSER, W., BAERENDS, E. J. & ROS, P. (1980). *Discuss. Faraday Soc. (Symp.)* **14**, 211–234.

International Tables for X-ray Crystallography (1974). Vol. IV. Birmingham: Kynoch Press.

JONES, L. H., MCDOWELL, R. S. & GOLDBLATT, M. (1969). *Inorg. Chem.* **8**, 2349–2363.

LA PLACA, S. J., HAMILTON, W. C., IBERS, J. A. & DAVISON, A. (1969). *Inorg. Chem.* **8**, 1928–1935.

LEHMANN, M. S. & LARSEN, F. K. (1974). *Acta Cryst.* A**30**, 580–584.

LEVENSON, R. A. & GRAY, H. B. (1975). *J. Am. Chem. Soc.* **97**, 6042–6047.

MCKINNEY, R. J. & PENSAK, D. A. (1979). *Inorg. Chem.* **18**, 3413–3417.

MCLEAN, A. D. & YOSHIMINE, M. (1967). *Tables of Linear Molecular Wave Functions.* Suppl. to *IBM J. Res. Dev.* **11**.

MITSCHLER, A., REES, B. & LEHMANN, M. S. (1978). *J. Am. Chem. Soc.* **100**, 3390–3397.

QUICKSALL, C. O. & SPIRO, T. G. (1969). *Inorg. Chem.* **8**, 2363–2367.

RANSIL, B. J. (1960). *Rev. Mod. Phys.* **32**, 239–244.

REES, B. (1976). *Acta Cryst.* A**32**, 483–488.

REES, B. (1978). *Acta Cryst.* A**34**, 254–256.

REES, B. & MITSCHLER, A. (1976). *J. Am. Chem. Soc.* **98**, 7918–7924.

REES, B. & WIEST, R. (1981). To be published.

SAVARIAULT, J. M. (1978). Private communication.

SHOEMAKER, D. P. (1968). *Acta Cryst.* A**24**, 136–142.

WATSON, R. E. & FREEMAN, A. J. (1961). *Acta Cryst.* **14**, 27–37.

Acta Cryst. (1982). B**38**, 15–20

Neutron Diffraction Refinement of Pyroelectric Lithium Perchlorate Trihydrate

BY JAN-OLOF LUNDGREN, RUNE LIMINGA AND ROLAND TELLGREN

Institute of Chemistry, University of Uppsala, Box 531, *S*-751 21 *Uppsala, Sweden*

(*Received* 16 *February* 1981; *accepted* 12 *May* 1981)

Abstract

The crystal structure of pyroelectric lithium perchlorate trihydrate has been refined from neutron diffraction data, corrected for thermal diffuse scattering. $LiClO_4.3H_2O$, FW 160·436, hexagonal, $P6_3mc$, a = 7·7192 (4), c = 5·4531 (5) Å, V = 281·40 Å^3, Z = 2 [Chomnilpan, Liminga & Tellgren (1977). *Acta Cryst.* B**33**, 3954–3957]; D_x = 1·89, D_m = 1·89 Mg m^{-3}, μ(measured) = 0·23 mm^{-1}, λ = 1·210 Å. Refinement based on 1284 data recorded at 294 K from a spherical crystal gave a final $R_w(F^2)$ value of 0·048. The intensity data were severely affected by extinction. Refinements using several extinction models showed that significant differences in the thermal parameters were obtained in all refinements. The changes in the positional parameters were not significant. The ClO_4^- ion was found to be slightly asymmetric: the Cl–O bond directed along the polar c axis is 1·428 (1) Å compared to the value 1·439 (1) Å for the other three Cl–O bonds, which are equivalent by symmetry.

0567-7408/82/010015-06$01.00